$^3\Sigma_u^+$ bound and continuum states in e^--He_2^+ scattering

Brendan M. McLaughlin
Institute for Theoretical Atomic and Molecular Physics, Harvard-Smithsonian Center for Astrophysics, 60 Garden Street, Cambridge, Massachusetts 02138

Charles J. Gillan* and Philip G. Burke
Department of Applied Mathematics and Theoretical Physics, The Queen's University of Belfast, Belfast BT7 1NN, United Kingdom

John S. Dahler
Department of Chemistry and Department of Chemical Engineering and Materials Science, University of Minnesota, Minneapolis, Minnesota 55455

(Received 12 June 1992; revised manuscript received 3 September 1992)

Ab initio calculations are performed on the e^--He_2^+ complex using the R-matrix technique. A two-state approximation is utilized in which the $X\ ^2\Sigma_u^+$ and the $A\ ^2\Sigma_g^+$ electronic states of He_2^+, in the close-coupling expansion, are represented by truncated configuration-interaction (CI) wave functions obtained from multiconfiguration-self-consistent-field–complete-active-space-SCF (MCSCF-CASSCF) calculations. A $(4s,2p,2d)$ Slater basis is used to perform bound-state calculations at SCF, full CI, and MCSCF-CASSCF levels, to gauge the quality of wave functions at various bond separations. Elastic cross sections are presented for selected bond lengths in the range 1.5–4.0a_0, for the $^3\Sigma_u^+$ total symmetry. $He_2^*(1\sigma_g 1\sigma_u^2 np\sigma$ and $nf\sigma\ ^3\Sigma_u^+)$ resonances are detected at each separation and fitted to Breit-Wigner formulas in order to determine their energies and autoionization widths. In addition, low-lying $He_2^*(1\sigma_g^2 1\sigma_u ns, nd$, and $ng\ ^3\Sigma_u^+)$ bound states are also calculated at several geometries.

PACS number(s): 34.80.Bm, 31.20.Tz, 31.20.Di, 34.90.+q

I. INTRODUCTION

In this paper we report results of *ab initio* calculations for the low-energy elastic scattering of electrons from He_2^+ molecular ions. To our knowledge no other methods have been used for scattering calculations on this system nor have there been experimental measurements of the process; this is due, no doubt, to the difficulty of handling He_2^+ in the laboratory. He_2^+ ions produced from neutral dimers are normally in hot vibrational and rotational states and therefore must be quenched in order to perform experiments on the ground vibrational state [1]. We report in this work *ab initio* calculations of cross sections for elastic scattering and, in addition, autoionization widths are obtained for several bond lengths. There are no relevant experimental data or theoretical work with which to compare our results at this time.

Estimates for the autoionization widths arising from the interaction of two metastable helium atoms in their triplet states have been reported previously by Garrison, Miller, and Schaefer [2]. We note that only approximate estimates of the autoionization widths and resonance widths for the high-lying states $^1\Sigma_g^+$, $^3\Sigma_u^+$, and $^5\Sigma_g^+$ of He_2^* have been made. For these states of the helium dimer Garrison, Miller, and Schaefer [2] parametrized the autoionization widths as exponentially decaying functions of internuclear separation, as opposed to calculating them from first principles. As noted by Müller *et al.* [3], detailed knowledge of the $^3\Sigma_u^+$ and $^1\Sigma_g^+$ resonances widths as functions of internuclear separation are required to fully understand the energy spectrum of electrons produced by ionizing collisions between pairs of metastable He($2\ ^1S, 2\ ^3S$) atoms. Autoionization is spin forbidden for the $^5\Sigma_g^+$ entrance channel, which may only be accessed through spin-orbital coupling, and so this symmetry may be neglected as indicated by Hill and coworkers [4].

The computations reported here open the way to a host of related theoretical problems [5,6]. From here we can progress to a detailed study of Penning and associative ionization in He*-He, and He*-He* collisions, with and without the presence of a photon field. Field-free associative ionization and excitation transfer cross sections have previously been studied, within a diabatic representation of the He*-He complex, using a multistate curve crossing model [7]. Bieniek, Müller, and Movre [8] recently have investigated associative and Penning ionization in He($2\ ^3S$)-He($2\ ^3S$) collisions using a uniform semiclassical approximation. There also have been recent experimental and theoretical studies by Müller *et al.* [9] on He*-He* collisions at thermal and subthermal kinetic energies.

Estimates have been made by Julienne and Mies [10] of the upper and lower bounds for the rate coefficient of Penning ionization in He($2\ ^3S$)–He($2\ ^3S$) collisions, which are respectively 10^{-9} and 5×10^{-11} cm^3 s^{-1}. Within the past two years Weiner, Masnou-Seeuws, and Giusti-Suzor [11] have published an extensive review of associative ionization in several systems and Niehaus [12] has reviewed field-free spontaneous electron emission from slow

atomic collisions at incident energies less than 10 keV. Finally, a review of field-free chemi-ionization in binary collisions at thermal energies has been made by Klucharev and Vujnović [13].

Our work will make it possible to study photoionization of the excited states of the helium dimer for which there are resonances in the resulting cross sections. These resonances can be analyzed and identified with Rydberg states of He_2^* from phase-shift calculations in e^--He_2^+ scattering. It then may be possible to resolve the controversy that exists at present in experiments on photon-assisted He*-He collisions [14,15].

We note that in models of the ejecta of the supernova SN 1987A [16], He^+ ions formed by the radioactive decay of ^{56}Co are removed by radiative and dielectronic recombination, charge transfer, the radiative association process $He^+ + He \rightarrow He_2^+ + h\nu$, and by reactions with CO. It is desirable to know accurately cross sections as well as rate constants for these processes. In particular, radiative recombination cross sections and rate coefficients may be obtained from *ab initio* photoionization cross sections calculations on the ground and excited states of the helium atom [17]. Quantitative calculations of the autoionization widths and resonance widths $\Gamma(R)$, as functions of the internuclear separation variable R, will permit a detailed investigation to be conducted of the dissociative recombination (DR) process, $e^- + He_2^+ \rightarrow He^* + He$. Generally it is recognized that the $^3\Sigma_g^+$ and $^1\Sigma_g^+$ are the two lowest-lying electronic states that provide the primary routes for DR but other diabatic states of the helium dimer, namely, $^3\Pi_u$, $^1\Pi_u$, $^3\Sigma_u^+$, and $^1\Sigma_u^+$ are possible routes [18]. Finally it is our intention to study vibrational excitation of the ground electronic state of the He_2^+ molecular ion, which will provide a rich source of information on this molecular-ion complex.

II. COMPUTATIONAL METHOD

A. Outline of calculations

We have applied the R-matrix method to the electron-molecular ion complex as outlined by Gillan [19] and McLaughlin *et al.* [5] in order to solve the scattering equations. For the solution of the scattering equations in the external region, specific to neutral molecular complexes, the reader should consult the work of Gillan *et al.* [20]. This R-matrix method has proved, among others, to be very successful in *ab initio* studies of low-energy electron molecule collisions. In particular, Tennyson, Noble, and Salvini [21] and Tennyson and Noble [22] applied the method to the e^--H_2^+ system, this work being extended by Shimamura, Noble, and Burke [23] to complete a detailed study of the Feshbach resonances converging to the first excited state. Recent work on the e^--H_2^+ and the e^--HeH^+ system, using the multichannel quantum-defect theory (MQDT) approach, within the R-matrix context, has also been carried out, respectively, by Branchett and Tennyson [24] and Sarpal and Tennyson [25]. Branchett and Tennyson [24] have augmented the work of Shimamura, Noble, and Burke [23] using the R-matrix method to compute transition dipole moments between low-lying bound and diffuse Rydberg states of the H_2 molecule. Tennyson [26] has used the R-matrix method to study bound and continuum states of the e^--CH^+ system. Sarpal *et al.* [27] have completed work on bound states of the e^--HeH^+ system and have implemented the method of Seaton [28] to calculate the lowest 33 bound electronic states of the HeH molecule. We have used the same technique here for the bound states of the He_2^* complex.

The next three sections cover the most important aspects of our cross-section calculations of the scattering process. We begin by considering the representation of the target-state wave functions. Following this we describe the method of solution of the scattering equations and conclude with a brief discussion of our choice of the $\mathcal{L}^2$ functions which are important constituents of the R-matrix basis states.

B. Target wave-function calculations

The target eigenstates are expanded in a set of orthogonal molecular orbitals, each of which is expanded in a basis of Slater-type orbitals (STO's). All the calculations have been performed using the (4*s*, 2*p*, 2*d*) double ζ plus polarization (DZ+P), STO basis of Reagen, Browne, and Matsen [29]. The sensitivity of the scattering calculations to the target representations has previously been demonstrated by McLaughlin *et al.* [6] using (SCF and full CI) approximations for the target states.

The present study began with a self-consistent-field (SCF) calculation of the $1\sigma_g^2 1\sigma_u^1\, X\,^2\Sigma_u^+$ state of He_2^+ in the STO basis. Due to linear dependence we were forced to delete one of the σ_g and one of the σ_u basis functions. This yielded the orbital set

$$1\sigma_g \rightarrow 6\sigma_g, \quad 1\sigma_u \rightarrow 6\sigma_u, \quad 1\pi_u \rightarrow 3\pi_u, \quad 1\pi_g \rightarrow 3\pi_g, \quad 1\delta_g, \quad 1\delta_u . \tag{1}$$

We then Schmidt orthogonalized the open-shell virtual orbitals to the bound orbitals and used the resulting orthogonal orbital set for the expansion of both target states.

Our first approximation was to use single configurations for both the $X\,^2\Sigma_u^+$ and $A\,^2\Sigma_g^+$ states. The X state was represented by its SCF form. We found that the representation of the A state in the common orbital basis was close to that obtained from a SCF calculation on the A-state configuration itself. The second approximation began with full configuration-interaction (CI) calculations [30] for both target states in the common orbital set defined by (1). The dimension of the configuration-state-function (CSF) space for each target eigenfunction was 562. This representation was, therefore, at the STO basis-set limit and independent of the form of representation of the molecular orbitals that we had chosen. Using these target-state expansions would have rendered the solution of the scattering equations difficult due to the algorithm used in our codes for Hamiltonian matrix construction. We note in passing that this restriction has been removed.

In order to make the inner region Hamiltonian manageable it was necessary to reduce the number of

CSF's, without unduly degrading the wave functions. Accordingly, we evaluated the first-order spin-reduced density matrix for the X state (in the full CI approximation), diagonalized this, and then transformed the initial orbital set to natural orbitals, cf. Mulliken and Ermler [31]. The new orbital set was truncated by omitting all natural orbitals with occupation numbers less than 10^{-3}. The truncated natural orbital space was then

$$1\sigma_g \rightarrow 3\sigma_g \ , \quad 1\sigma_u \rightarrow 2\sigma_u \ , \quad 1\pi_u \ , \quad 1\pi_g \ . \tag{2}$$

The performance of a full CI calculation in set (2) yielded 30 CSF's per state with a negligible degradation in absolute energy compared with full CI in the orbital set (1). This can be seen from Table I. We found that the degradation in energy was larger for internuclear separations different from the equilibrium separation. Although the use of these natural orbitals derived from the ground state introduces an extra approximation in the expansion of the excited state, we do not believe that it significantly affects the results reported here.

In our full CI calculations performed with the SCF molecular-orbital set (1), at internuclear separations less than $R \lesssim 1.5a_0$, we found that the expansion coefficients of the SCF molecular orbitals became extremely large, an indication of severe linear dependence in the basis set. In the CI technique only configuration coefficients are varied since those of the molecular orbitals are already fixed. Our results were therefore judged to be untrustworthy at internuclear geometries less than $\lesssim 1.45a_0$ for the A state using this CI procedure and have not been included here. The X state results are in satisfactory agreement with the work of Kahn and Jordan [32] and are reported for bond separation $R \geq 1.3a_0$.

To circumvent these problems one must use the complete active-space self-consistent field (CASSCF) with the multiconfiguration self-consistent-field (MCSCF) procedure [33,34], or a variant of this approach, for which

TABLE I. Comparison of the truncated natural orbital CI approximation, with full CI at selected bond separations for the target energies of the X and A electronic states of He_2^+. The $(4s,2p,2d)$ STO basis of Reagen, Browne, and Matsen [29] is used. All the energies are given in hartrees.

R (units of a_0)	Truncated CI $X\,^2\Sigma_u^+$ state	Full CI $X\,^2\Sigma_u^+$ state
1.5	−4.922 291 5	−4.930 279 4
2.0	−4.982 802 2	−4.990 725 8
2.5	−4.968 760 5	−4.976 836 1
3.0	−4.943 661 9	−4.951 917 3
3.5	−4.923 105 4	−4.931 538 0
4.0	−4.889 604 1	−4.917 716 2
R (units of a_0)	$A\,^2\Sigma_g^+$ state	$A\,^2\Sigma_g^+$ state
1.5	−4.195 363 5	−4.208 052 8
2.0	−4.594 455 0	−4.604 711 1
2.5	−4.757 254 5	−4.766 982 9
3.0	−4.827 267 8	−4.836 745 1
3.5	−4.859 095 2	−4.868 413 3
4.0	−4.850 456 0	−4.883 517 8

both configuration and molecular-orbital coefficients are optimized. Using the CASSCF procedure one gets better orbitals automatically. However, in the case of this $(4s,2p,2d)$ Slater basis there still are problems if one uses the entire set for the $^2\Sigma_u^+$ and $^2\Sigma_g^+$ symmetries at internuclear geometries near the united atom limit ($R \rightarrow 0$), where there is severe linear dependence. The main attraction of this $(4s,2p,2d)$ Slater basis is the advantage it provides of doing CASSCF on the whole orbital set (1), as opposed to a subset, which is the normal way structure calculations are performed when very large Slater basis sets are employed. We note that here the MCSCF-CASSCF and the full CI approximations are functionally equivalent which we confirmed for our own satisfaction, by performing calculations in both approximations. Further details may be obtained from the authors for the interested reader. The full CI results were obtained using a modified version of the ALCHEMY I codes [35,36]. The MCSCF-CASSCF results were obtained using the ALCHEMY II suite of codes [37]. Following the work of Branchett and Tennyson [38] we carefully checked the integration grids used in this work. An additional complication which may arise in scattering calculations is an inconsistency in phase between the scattering and target-wave functions. This was pointed out by Noble [39] who modified the algorithm to remove this inconsistency. This modification has now been incorporated in the R-matrix suite of programs.

C. The scattering calculation

All of the calculations reported here have been performed with the nuclei held fixed in space. In the fixed nuclei R-matrix theory there are two regions of Euclidean configuration space. The inner region is a hypersphere defined by $r_i < a \ \forall i$, where r_i is the radial distance of electron i from the center of mass of the target. The outer region in the electron-scattering problem for an N electron target is defined by $r_i < a$ for $i = 1,N$ and $r_{N+1} > a$. The parameter a is the R-matrix radius, which we have chosen to be $10a_0$, a value large enough that the target-state charge distributions are enveloped by the hypersphere. Electron exchange is neglected in the outer region. A multicenter configuration-interaction-type expansion of the scattering wave function is chosen to represent the e^--He_2^+ complex in the finite inner region. Thus, the inner-region wave function is expanded in the basis

$$\psi_k(\mathbf{x}_1,\mathbf{x}_2,\mathbf{x}_3,\mathbf{x}_4) = \mathcal{A} \sum_{ij} \bar{\phi}_i(\mathbf{x}_1,\mathbf{x}_2,\mathbf{x}_3,\sigma_4)\eta_j(\mathbf{r}_4)\alpha_{ijk} + \sum_j \chi_j(\mathbf{x}_1,\mathbf{x}_2,\mathbf{x}_3,\mathbf{x}_4)\beta_{jk} \ , \tag{3}$$

where $\mathcal{A}$ is the antisymmetrization operator and $\mathbf{x}_i = (\mathbf{r}_i,\sigma_i)$ stands for the space and spin coordinates of the ith electron. The functions $\bar{\phi}_i$ are eigenfunctions of the total spin operator S^2 and its z component S_z, formed by coupling the products of the spin function of the continuum electron with the target electronic states ϕ_i. The η_j functions are continuum molecular orbitals which are

nonzero on the boundary of the inner region. The second summation is over square integrable $\mathcal{L}^2$ functions, χ_j, descriptive of states with all of the electrons in bound orbitals. The composition of this second summation is discussed in the following section. We have retained in Eq. (3) the lowest two states of the He_2^+ molecular ion, namely the $X\,^2\Sigma_u^+$ ground state and $A\,^2\Sigma_g^+$ excited state. These two-state calculations reported here will serve as a comparison for future multistate calculations on this system. The coefficients α_{ijk} and β_{jk} are determined by diagonalizing the operator $(H+L)$ in the basis ψ_k in the inner region. Thus

$$\langle \psi_k | H+L | \psi_j \rangle = E_k \delta_{kj} , \tag{4}$$

where H is the electronic Hamiltonian for the target plus projectile and L, a surface projection operator introduced by Bloch [40], is so defined that $(H+L)$ is Hermitian. The construction and diagonalization of the operator $(H+L)$ in the inner region is carried out using a modified, machine portable, version of the IBM ALCHEMY quantum chemistry program suite [35,36].

The continuum molecular orbitals η_j, representing the scattered electron, are formed by taking suitable linear combinations of the target molecular orbitals and additional continuum basis functions, the radial parts of which are obtained by numerically solving the model scattering problem

$$\left[\frac{d^2}{dr^2} - \frac{l_i(l_i+1)}{r^2} + 2V_0(r) + k_j^2 \right] u_{ij}(r) = 0 \tag{5}$$

subject to the fixed boundary conditions

$$u_{ij} = 0 , \quad \left[\frac{a}{u_{ij}(r)} \frac{du_{ij}(r)}{dr} \right]_{r=a} = 0 . \tag{6}$$

Here V_0 is the spherical part of the static potential of the SCF target ground state of He_2^+. The use of the fixed boundary condition requires the introduction of the Buttle correction [41] when computing the R matrix. Four partial waves were used for each continuum symmetry. Convergence was achieved with three partial waves per continuum symmetry. We chose the continuum basis to be complete up to 11 Ry, a condition that required the use of about nine continuum functions per partial wave.

The outer-region part of the collision problem was handled by adopting a single-center, no-exchange, close-coupling expansion of the wave function. R-matrix propagator [42] and accelerated Gailitis expansion methods [43] were employed in the solution. For the scattering process the external region was solved for positive energies and the R matrix matched onto outgoing wave solutions. The T matrices obtained by this procedure then were employed in standard formulas to produce differential and integral cross sections. To evaluate bound states of He_2^* we employed the method of Seaton [28], as used by Sarpal *et al.* [27] for HeH*. In our earlier work [6] we reported on the bound-state energy of the $He_2(1\sigma_g^2 1\sigma_u 2s\, a\,^3\Sigma_u^+)$ state, which was evaluated by solving the collision problem with all channels closed. The advantage of the R-matrix method is that the bound states can be obtained as an external region scattering problem with negative kinetic energy and requires no reevaluation of the inner region.

D. The $\mathcal{L}^2$ functions for full CI target representations

For scattering calculations with a full CI representation of the target states the truncated natural orbital set of Eq. (2) was used. To ensure consistency with the use of full CI the $\mathcal{L}^2$ terms consisted of all possible arrangements of four electrons in the natural orbital space. Our scattering calculation was therefore completely correlated within this truncated orbital space. Naturally, only those configurations which are consistent with the target symmetry and equivalence restrictions of the scattering symmetry in question were constructed.

III. RESULTS AND DISCUSSION

Very little scattering information is available for this molecular system. This is probably due to several anomalies in target wave-function representation at various internuclear separations. Figure 1 shows several low-lying potential-energy curves of He_2^+ taken from the valence-bond calculations of Michels [44] in the adiabatic representation. The avoided crossings in the $^2\Sigma_g^+$ symmetries are clearly visible at bond separations $R \lesssim 1.5a_0$, as in the recent work of Metropoulos, Nicolaides, and Buenker [45]. In the diabatic regime the $A\,^2\Sigma_g^+$ state correlates in the united atom limit $(R \to 0)$ to the $Be^+(1s2p^2)$ state [46,47]. At internuclear separations greater than approximately $6.0a_0$ the $A\,^2\Sigma_g^+$ and the $X\,^2\Sigma_u^+$ states become degenerate. For bond lengths greater than the equilibrium geometry r_e there is a relatively large energy separation between the $A\,^2\Sigma_g^+$ state and higher-lying $^2\Sigma_{g,u}^+$ or $^2\Pi_{g,u}$ states. This justifies our use of a two-state calculation for this system. Shimamura, Noble, and Burke [23] successfully employed a similar two-state approximation in their work on the e^--H_2^+ complex.

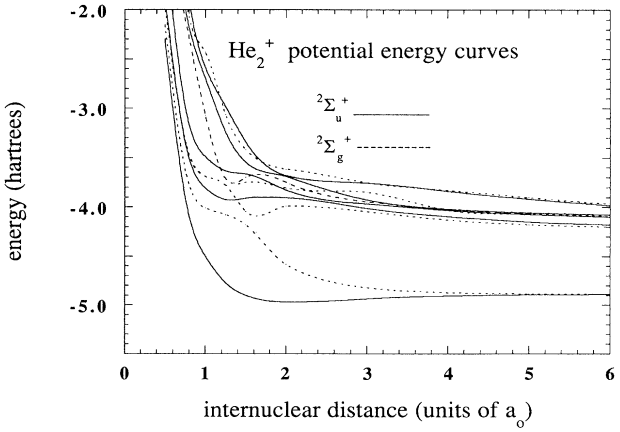

FIG. 1. He_2^+ potential-energy curves for low-lying $^2\Sigma_u^+$ and $^2\Sigma_g^+$ states from the valence-bond calculations of Michels [44]. The avoided crossings in the $^2\Sigma_g^+$ symmetries are clearly visible at bond separations $R \lesssim 1.5a_0$. The $^2\Pi_{g,u}$ states have been omitted in the graph for the sake of clarity.

Figure 2 shows the potential-energy curves we calculated for the X and A target states of the He_2^+ molecular ion using the SCF approximation. For comparison purposes the accurate multiconfiguration self-consistent-field (MCSCF) results [32] are shown for these same two states. At the SCF level the single-configuration representation of the A state is inadequate near the united atom limit ($R \rightarrow 0$) and gives no avoided crossing in the $A\ ^2\Sigma_g^+$ state at internuclear separations for the range $1.0-1.5a_0$. The curves shown in Figs. 2 and 3 incorporate the correction to the Kahn and Jordan [32] data that was pointed out by Yu and Wing [48] for the $^2\Sigma_u^+$ ground state.

The energies of the X and A states of He_2^+ in both the MCSCF-CASSCF and the full CI approximations are identical to six decimal places for $R \gtrsim 1.45a_0$, using the $(4s,2p,2d)$ Slater basis. Consequently we have chosen to plot only the MCSCF-CASSCF results in Fig. 3. For comparison purposes the results of Kahn and Jordan [32] are included in both these figures. In both the MCSCF-CASSCF and full CI calculations, using the $(4s,2p,2d)$ Slater basis of Reagen, Browne, and Matsen [29], the severe linear dependence in the basis set for internuclear geometries $R \lesssim 1.45a_0$ gives erroneous results for the A state. These are not reported here. The X-state results agree well with the work of Kahn and Jordan [32] and are given for bond separations $R \geq 1.3a_0$. Our scattering work requires the use of a common set of molecular orbitals to represent both the X and A states. One therefore can only use this $(4s,2p,2d)$ Slater basis for scattering work at bond separations greater than $R \gtrsim 1.5a_0$.

It is worth noting that for internuclear distances $R \geq 1.5a_0$ the SCF-MO-LCAO wave functions provide qualitatively satisfactory representations of the X and the A states of He_2^+. These single-configuration SCF wave functions belong to the valence configuration-interaction (VCI) [31] category and therefore automatically dissociate into the correct Hartree-Fock states of the molecular ion. Our full CI and MCSCF-CASSCF calculations at bond separations $R \geq 1.5a_0$ are in excellent agreement with previous work. In particular, for the $X\ ^2\Sigma_u^+$ ground state there is good agreement with the larger basis set calculations of Sunil *et al.* [49], Kahn and Jordan [32], Yu and co-workers [50,51] and Bauschlicher, Partridge, and Ceperley [52]. A useful indication of the accuracy of the wave function for the X state is provided by comparing the value obtained for the dissociation constant D_e at the equilibrium bond length r_e with values available in the literature. Our results presented in Table II for the dissociation constant D_e and the equilibrium bond separation r_e are in harmony with the theoretical and experimental values of previous studies. There is no comparable test for the repulsive A state and so one must rely solely upon the results of previous calculations for comparisons.

Earlier scattering results on this system were carried out by McLaughlin *et al.* [5], who performed cross-section calculations at two fixed internuclear separations, $1.8a_0$ and $2.0625a_0$, using the same two-state approximation as we have used here. The present work is an extension of this earlier work to selected bond separations in the region 1.5–$4.0a_0$, using full CI target-state representations obtained from the natural orbitals CASSCF calculations. As in our previous studies the direct potential in the outer-region calculations contains, in addition to the dominant Coulomb term, contributions from the ground- and excited-state quadrupole moments as well as the dipole moment coupling the X and A states.

Work on electron collisions with CH^+ by Tennyson [26], H_2^+ by Shimamura, Noble, and Burke [23] and HeH^+ by Sarpal, Tennyson, and Morgan [53] has shown that complex multichannel quantum defects (MCQD) are useful in analyzing complicated resonance structure and superexcited states. The T matrix above a threshold can be used to calculate the MCQD parameters, $\mu_n = \alpha_n + i\beta_n$ as outlined by Seaton [54]. Here α_n is re-

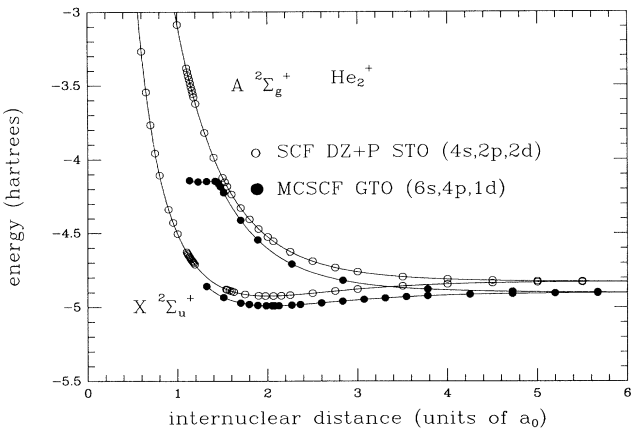

FIG. 2. Comparisons of the SCF potential-energy calculations using the $(4s,2p,2d)$ Slater basis for the X and the A states of He_2^+ with MCSCF $(6s,4p,1d)$ Gaussian-basis calculations of Kahn and Jordan [32]. Note the failure of the SCF calculations to represent the avoided crossing in the $He_2^+(1\sigma_g 1\sigma_u^2\ A\ ^2\Sigma_g^+)$ state.

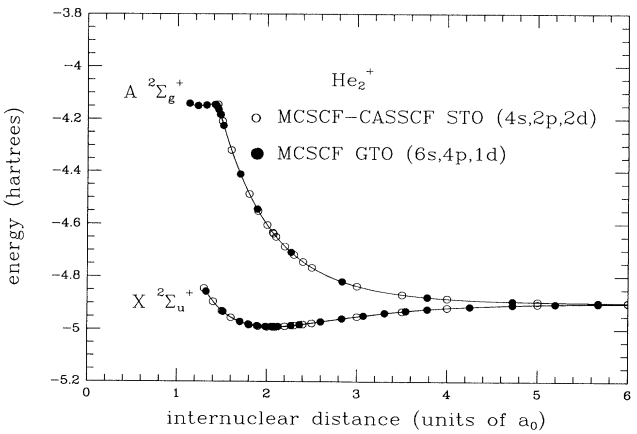

FIG. 3. MCSCF-CASSCF potential-energy calculations for the X and A states of He_2^+ using the $(4s,2p,2d)$ Slater basis compared with the MCSCF $(6s,4p,1d)$ Gaussian basis calculations of Kahn and Jordan [32].

TABLE II. The dissociation energy D_e (eV) and the equilibrium internuclear separation r_e (a_0). The calculated values from our target representations are compared with existing ones for the ground state of $He_2^+(1\sigma_g^2 1\sigma_u\, X\,^2\Sigma_u^+)$.

Method	D_e (eV)	r_e (units of a_0)
SCF-GTO (Maas *et al.* [62])	2.622	2.0050
SCF-STO (present work)	2.648	2.0057
CI-GTO (Maas *et al.* [62])	2.459	2.0457
MCSCF-GTO (Kahn and Jordan [32])	2.451	2.0447
CI-STO (Liu [63])	2.469±0.006	2.0440
CI-GTO/STO (Bauschlicher, Partridge, and Ceperley [51])	2.469+0.003	2.0428
CI-STO (present work)	2.521	2.0444
MCSCF-CASSCF-STO (present work)	2.521	2.0444
Expt. estimates (Huber and Herzberg [64])	2.34 and 2.55	2.0424
Expt. estimates (Ginter and Ginter [65])	2.33±0.02	2.0423

lated to the effective quantum number n^* by $\alpha_n = n - n^*$ and β_n is defined as $\beta_n = \frac{1}{4}\Gamma_n (n^*)^3$, with Γ_n being the width of the resonance n. The effective quantum number n^* is obtained from the relation

$$\varepsilon_n = \varepsilon_\infty - \frac{1}{(n^*)^2} , \tag{7}$$

where ε_∞ is the series limit and ε_n the energy of the resonance n.

The resonances in the cross sections shown in Fig. 4 were detected and fitted to the following Breit-Wigner form for several overlapping resonances:

$$\eta(\varepsilon) = \eta_0(\varepsilon) + \sum_{i=1}^{M} \tan^{-1} \frac{\Gamma_i}{2(\varepsilon_n^i - \varepsilon)} . \tag{8}$$

Here $\eta_0(\varepsilon)$ is the background phase shift at scattering energy ε, ε_n^i the position of the ith resonance, Γ_i the width, and M the number of overlapping resonances. The resonances were fitted automatically using a modified version of the computer code of Tennyson and Noble [55,56], with a quadratic form for the background phase shift $\eta_0(\varepsilon)$, using an energy mesh of 10^{-5} Ry. From an analysis of the eigenphase sum obtained from the K matrix, the effective quantum number n^*, the complex quantum defect $\mu_n = \alpha_n + i\beta_n$, and the autoionizing width were obtained for low-lying resonances at each fixed internuclear separation. The fitted parameters from our scattering results are presented in Tables III–X. The results are for several low-lying He_2 ($1\sigma_g 1\sigma_u^2 np\sigma\, ^3\Sigma_u^+$ and $1\sigma_g 1\sigma_u^2 nf\sigma\, ^3\Sigma_u^+$) quasibound states that contribute to the elastic scattering cross section at selected bond lengths in the range 1.5–$4.0a_0$.

Our results indicate that the following resonance processes contribute to the elastic-scattering process in the $^3\Sigma_u^+$ symmetry:

$$\begin{aligned} &e^- + He_2^+(1\sigma_g^2 1\sigma_u X\,^2\Sigma_u^+) \\ &\qquad\downarrow \\ &He_2(1\sigma_g 1\sigma_u^2 np\sigma, nf\sigma, nh\sigma, \ldots, ^3\Sigma_u^+) \\ &\qquad\downarrow \\ &He_2^+(1\sigma_g^2 1\sigma_u X\,^2\Sigma_u^+) + e^- . \end{aligned} \tag{9}$$

Each corresponds to a rearrangement of the He_2^+ molecular-ion core with the continuum electron attaching itself to the repulsive unstable excited $A\,^2\Sigma_g^+ He_2^+$ state. These quasibound states, therefore, consist of an unstable excited He_2^+ core surrounded by and interacting with a diffuse Rydberg orbital. Our results clearly show that there are several resonance series in the elastic-scattering cross sections. The most prominent of these is the $np\sigma$ series and the weaker is the $nf\sigma$. A very faint $nh\sigma$ series is visible at internuclear distances greater than $2.0a_0$. Only the $np\sigma$ and $nf\sigma$ series have been analyzed in detail here.

In common with the work of Shimamura, Noble, and Burke [23] on superexcited states of H_2 we have analyzed the real and imaginary parts of the quantum defects for these superexcited states of He_2. Figures 5 and 6 show the real and imaginary parts of the quantum defects for the $He_2(1\sigma_g 1\sigma_u^2 np\sigma$ and $nf\sigma\, ^3\Sigma_u^+)$ series. The behavior of the real part of μ_n for both the $np\sigma$ and $nf\sigma$ shows trends similar to those appearing in Fig. 4 of Ref. [23] for H_2. The imaginary part of μ_n for our $nf\sigma$ series behaves similarly to results reported by Shimamura, Noble, and Burke [23] on superexcited states of H_2. However, our $np\sigma$ series (except for the $3p\sigma$) results show structure which have no counterparts for H_2. Within the fixed nuclei approximation the Wigner–Von Neumann noncrossing rule applies. Therefore it is likely that these $np\sigma$ superexcited Rydberg resonance states exhibit avoided crossings. For completeness in Fig. 7 we show the absolute magnitudes of the quantum defects for the $np\sigma$ and $nf\sigma\, ^3\Sigma_u^+$ superexcited He_2 states as functions of the principal quantum number for the several internuclear separations.

The curves of Fig. 8 illustrate the $np\sigma$ and $nf\sigma\, ^3\Sigma_u^+$ autoionizing widths varying with internuclear distance. As before the $np\sigma$ and $nf\sigma\, ^3\Sigma_u^+$ resonance series behave differently. The $3p\sigma$ resonance vanishes at $R \geq 3.0a_0$, whereas the higher-lying members of the $np\sigma$ series are monotonically decreasing functions of internuclear distance. We attribute the structure in the autoionizing width of the $np\sigma$ series to the proximity of the avoided crossing in the $A\,^2\Sigma_g^+$ target state. The $nf\sigma\, ^3\Sigma_u^+$ autoionizing widths are monotonic increasing functions of

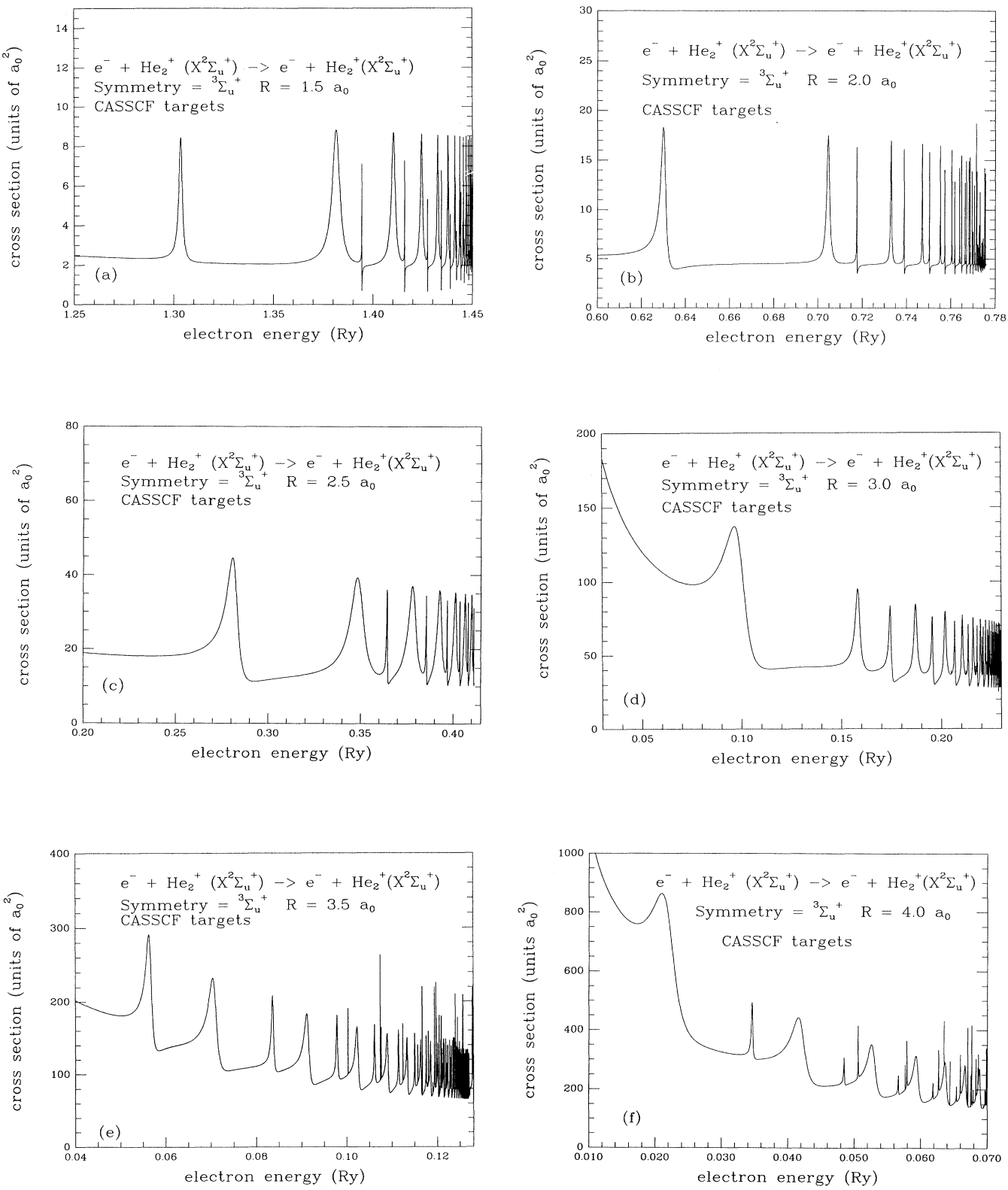

FIG. 4. Cross sections for elastic scattering as a function of the incident electron energy. The symmetry is $^3\Sigma_u^+$ and the bond separations are 1.5, 2.0, 2.5, 3.0, 3.5, and $4.0a_0$, (a)–(f), respectively. Correlated CI target wave functions obtained from natural orbital analysis of MCSCF-CASSCF calculations are used to represent the X and A states of the He_2^+ molecular ion. The prominent Rydberg series is the $np\sigma$; the weaker one is the $nf\sigma$; the very faint $nh\sigma$ series is also visible at the larger internuclear distances.

TABLE III. Effective quantum numbers (n^*), complex quantum defects ($\mu_n = \alpha_n + i\beta_n$), and positions ($\varepsilon_n$) of the $1\sigma_g 1\sigma_u^2 np\sigma$ and $1\sigma_g 1\sigma_u^2 nf\sigma$ resonances in the $^3\Sigma_u^+$ scattering symmetry. The position of the resonances are relative to the $X\,^2\Sigma_u^+$ state of He_2^+ at the fixed internuclear separation of $R = 1.5a_0$.

n	n^*	$\alpha_n = n - n^*$	$\beta_n = \mathrm{Im}(\mu)$	$\lvert\mu_n\rvert$	ε_n (Ry)
			$1\sigma_g 1\sigma_u^2 np\sigma\ ^3\Sigma_u^+$		
3	2.579 131 6	0.420 868 4	$0.882\,616\,1^{-2}$	0.420 960 9	1.303 523 4
4	3.721 729 4	0.278 270 6	$0.586\,406\,6^{-1}$	0.284 382 2	1.381 660 4
5	4.795 508 1	0.204 491 9	$0.621\,770\,1^{-1}$	0.213 735 6	1.410 371 8
6	5.831 472 7	0.168 527 3	$0.624\,588\,6^{-1}$	0.179 729 1	1.424 449 4
			$1\sigma_g 1\sigma_u^2 nf\sigma\ ^3\Sigma_u^+$		
4	4.102 761 6	−0.102 761 6	$0.100\,964\,6^{-2}$	0.102 766 6	1.394 447 6
5	5.133 556 0	−0.133 556 0	$0.135\,906\,7^{-2}$	0.133 562 9	1.415 910 1
6	6.147 886 5	−0.147 886 5	$0.157\,003\,8^{-2}$	0.147 894 8	1.427 398 4

TABLE IV. Effective quantum numbers (n^*), complex quantum defects ($\mu_n = \alpha_n + i\beta_n$), and positions ($\varepsilon_n$) of the $1\sigma_g 1\sigma_u^2 np\sigma$ and $1\sigma_g 1\sigma_u^2 nf\sigma$ resonances in the $^3\Sigma_u^+$ scattering symmetry. The position of the resonances are relative to the $X\,^2\Sigma_u^+$ state of He_2^+ at the fixed internuclear separation of $R = 2.0a_0$.

n	n^*	$\alpha_n = n - n^*$	$\beta_n = \mathrm{Im}(\mu)$	$\lvert\mu_n\rvert$	ε_n (Ry)
			$1\sigma_g 1\sigma_u^2 np\sigma\ ^3\Sigma_u^+$		
3	2.613 184 2	0.386 815 8	$0.117\,440\,6^{-1}$	0.386 994 0	0.630 254 3
4	3.724 982 9	0.275 017 1	$0.197\,145\,5^{-1}$	0.755 725 0	0.704 624 8
5	4.784 320 5	0.215 679 5	$0.148\,203\,4^{-1}$	0.216 188 1	0.733 006 6
6	5.812 687 6	0.187 312 4	$0.120\,557\,7^{-1}$	0.187 700 0	0.747 097 4
			$1\sigma_g 1\sigma_u^2 nf\sigma\ ^3\Sigma_u^+$		
4	4.112 702 6	−0.112 702 6	$0.182\,873\,1^{-2}$	0.112 717 4	0.717 572 8
5	5.146 333 9	−0.146 333 9	$0.246\,475\,1^{-2}$	0.146 354 7	0.738 936 7
6	6.162 180 2	−0.162 180 2	$0.284\,225\,0^{-2}$	0.162 205 1	0.750 359 5

TABLE V. Effective quantum numbers (n^*), complex quantum defects ($\mu_n = \alpha_n + i\beta_n$), and positions ($\varepsilon_n$) of the $1\sigma_g 1\sigma_u^2 np\sigma$ and $1\sigma_g 1\sigma_u^2 nf\sigma$ resonances in the $^3\Sigma_u^+$ scattering symmetry. The position of the resonances are relative to the $X\,^2\Sigma_u^+$ state of He_2^+ at the fixed internuclear separation of $R = 2.5a_0$.

n	n^*	$\alpha_n = n - n^*$	$\beta_n = \mathrm{Im}(\mu)$	$\lvert\mu_n\rvert$	ε_n (Ry)
			$1\sigma_g 1\sigma_u^2 np\sigma\ ^3\Sigma_u^+$		
3	2.661 848 1	0.338 151 9	0.032 302 8	0.339 691 3	0.281 877 4
4	3.676 473 0	0.323 527 0	0.106 169 9	0.340 502 2	0.349 028 1
5	4.742 280 3	0.257 719 7	0.135 235 4	0.291 046 5	0.378 546 3
6	5.780 574 9	0.219 425 1	0.145 721 3	0.263 404 8	0.393 085 4
			$1\sigma_g 1\sigma_u^2 nf\sigma\ ^3\Sigma_u^+$		
4	4.130 862 5	−0.130 862 5	$0.835\,222\,7^{-2}$	0.131 128 8	0.364 409 2
5	5.169 128 0	−0.169 128 0	$0.101\,357\,3^{-1}$	0.169 431 4	0.385 586 7
6	6.188 723 2	−0.188 723 2	$0.869\,215\,3^{-2}$	0.188 923 3	0.396 902 5

TABLE VI. Effective numbers (n^*), complex quantum defects ($\mu_n=\alpha_n+i\beta_n$), and positions (ε_n) of the $1\sigma_g 1\sigma_u^2 np\sigma$ and $1\sigma_g 1\sigma_u^2 nf\sigma$ resonances in the $^3\Sigma_u^+$ scattering symmetry. The position of the resonances are relative to the $X\,^2\Sigma_u^+$ state of He_2^+ at the fixed internuclear separation of $R=3.0a_0$.

n	n^*	$\alpha_n=n-n^*$	$\beta_n=\mathrm{Im}(\mu)$	$\lvert\mu_n\rvert$	ε_n (Ry)
			$1\sigma_g 1\sigma_u^2 np\sigma\,^3\Sigma_u^+$		
3	2.689 005 0	0.310 995 0	$0.779\,500\,3^{-1}$	0.320 615 2	0.094 489 9
4	3.670 893 0	0.329 107 0	$0.342\,607\,4^{-1}$	0.330 885 5	0.158 550 7
5	4.690 587 0	0.309 413 0	$0.498\,085\,8^{-1}$	0.313 396 4	0.187 336 9
6	5.707 450 8	0.292 549 2	$0.460\,544\,2^{-1}$	0.296 152 1	0.202 089 8
			$1\sigma_g 1\sigma_u^2 nf\sigma\,^3\Sigma_u^+$		
4	4.151 525 6	−0.151 525 6	$0.207\,237\,3^{-1}$	0.152 936 2	0.174 767 3
5	5.195 690 0	−0.195 690 0	$0.186\,293\,0^{-1}$	0.196 574 7	0.195 744 5
6	6.215 110 8	−0.215 110 8	$0.201\,095\,5^{-1}$	0.216 048 7	0.206 899 9

TABLE VII. Effective quantum numbers (n^*), complex quantum defects ($\mu_n=\alpha_n+i\beta_n$), and positions (ε_n) of the $1\sigma_g 1\sigma_u^2 np\sigma$ and $1\sigma_g 1\sigma_u^2 nf\sigma$ resonances in the $^3\Sigma_u^+$ scattering symmetry. The position of the resonances are relative to the $X\,^2\Sigma_u^+$ state of He_2^+ at the fixed internuclear separation of $R=3.5a_0$.

n	n^*	$\alpha_n=n-n^*$	$\beta_n=\mathrm{Im}(\mu)$	$\lvert\mu_n\rvert$	ε_n (Ry)
			$1\sigma_g 1\sigma_u^2 np\sigma\,^3\Sigma_u^+$		
4	3.740 929 5	0.256 907 1	$0.187\,497\,3^{-1}$	0.259 748 1	0.056 564 0
5	4.747 364 4	0.252 635 6	$0.145\,735\,8^{-1}$	0.253 055 6	0.083 649 9
6	5.758 166 2	0.241 833 8	$0.127\,495\,6^{-1}$	0.242 169 6	0.097 860 4
			$1\sigma_g 1\sigma_u^2 nf\sigma\,^3\Sigma_u^+$		
4	4.179 831 0	−0.179 831 0	$0.372\,205\,8^{-1}$	0.183 642 5	0.070 782 6
5	5.223 543 4	−0.223 543 4	$0.420\,188\,7^{-1}$	0.227 458 2	0.091 370 8
6	6.245 264 6	−0.245 264 6	$0.354\,131\,2^{-1}$	0.247 808 0	0.102 381 6

TABLE VIII. Effective quantum numbers (n^*), complex quantum defects ($\mu_n=\alpha_n+i\beta_n$), and positions (ε_n) of the $1\sigma_g 1\sigma_u^2 np\sigma$ and $1\sigma_g 1\sigma_u^2 nf\sigma$ resonances in the $^3\Sigma_u^+$ scattering symmetry. The position of the resonances are relative to the $X\,^2\Sigma_u^+$ state of He_2^+ at the fixed internuclear separation of $R=4.0a_0$.

n	n^*	$\alpha_n=n-n^*$	$\beta_n=\mathrm{Im}(\mu)$	$\lvert\mu_n\rvert$	ε_n (Ry)
			$1\sigma_g 1\sigma_u^2 np\sigma\,^3\Sigma_u^+$		
5	4.787 870 0	0.212 130 0	$0.546\,340\,2^{-2}$	0.212 200 3	0.034 673 4
6	5.792 937 1	0.207 062 9	$0.649\,891\,7^{-2}$	0.207 164 9	0.048 497 2
			$1\sigma_g 1\sigma_u^2 nf\sigma\,^3\Sigma_u^+$		
4	4.215 291 7	−0.215 291 7	$0.755\,283\,0^{-1}$	0.228 155 7	0.022 017 5
5	5.253 129 8	−0.253 129 8	$0.829\,921\,2^{-1}$	0.266 387 7	0.042 058 3
6	6.272 392 8	−0.272 392 8	$0.858\,344\,4^{-1}$	0.285 596 2	0.052 878 7

TABLE IX. Autoionization widths, in rydbergs, at selected bond separations for the $1\sigma_g 1\sigma_u^2 np\sigma$ resonances in the $^3\Sigma_u^+$ scattering symmetry. The results are from fitting the elastic eigenphase sum to the Breit-Wigner form for overlapping resonances. The eigenphase sums are obtained from scattering calculations of electrons on the $X\,^2\Sigma_u^+$ state of He_2^+ using two-state CI target wave functions, obtained from natural orbital analysis of MCSCF-CASSCF calculations.

R (units of a_0)	$3p\sigma$	$4p\sigma$	$5p\sigma$	$6p\sigma$
1.5	2.058^{-3}	4.550^{-3}	2.255^{-3}	1.260^{-3}
2.0	2.632^{-3}	1.526^{-3}	5.413^{-4}	2.455^{-4}
2.5	6.851^{-3}	8.546^{-3}	5.072^{-3}	3.017^{-3}
3.0	1.604^{-2}	2.772^{-3}	1.930^{-3}	9.908^{-4}
3.5		1.432^{-3}	5.448^{-4}	2.671^{-4}
4.0			1.991^{-4}	1.337^{-4}

TABLE X. Autoionization widths, in rydbergs, at selected bond separations for the $1\sigma_g 1\sigma_u^2 nf\sigma$ resonances in the $^3\Sigma_u^+$ scattering symmetry. The results are from fitting the elastic eigenphase sum to the Breit-Wigner form for overlapping resonances. The eigenphase sums are obtained from scattering calculations of electrons on the $X\,^2\Sigma_u^+$ state of He_2^+ using two-state CI target wave functions, obtained from natural orbital analysis of MCSCF-CASSCF calculations.

R (units of a_0)	$4f\sigma$	$5f\sigma$	$6f\sigma$
1.5	5.848^{-5}	4.018^{-5}	2.702^{-5}
2.0	1.052^{-4}	7.233^{-5}	4.858^{-5}
2.5	4.739^{-4}	2.935^{-4}	1.467^{-4}
3.0	1.158^{-3}	5.313^{-4}	3.350^{-4}
3.5	2.038^{-3}	1.179^{-3}	5.815^{-4}
4.0	4.034^{-3}	2.290^{-3}	1.391^{-3}

R, due to couplings with a larger number of channels. This, again, is similar to the behavior of the superexcited states of H_2 [23].

We note that in the basis-set quantum chemistry approach the evaluation of Rydberg states is treated by incorporating diffuse orbitals into the basis set. This leads to severe linear dependence and therefore to a poor representation of the high-lying molecular Rydberg states. The inner-region R-matrix technique can be interpreted as merely a configuration-interaction approach which uses numerical basis functions with appreciable magnitudes on the R-matrix boundary. Diffuse Rydberg states that extend beyond the R-matrix boundary are accounted for by solving the coupled differential equations (for negative-scattering energies) in the outer region. We note that Tennyson and co-workers [27,24,53,25] and Norcross and Gorczyca [57,58] have illustrated the power of the quantum-defect and close-coupling method in

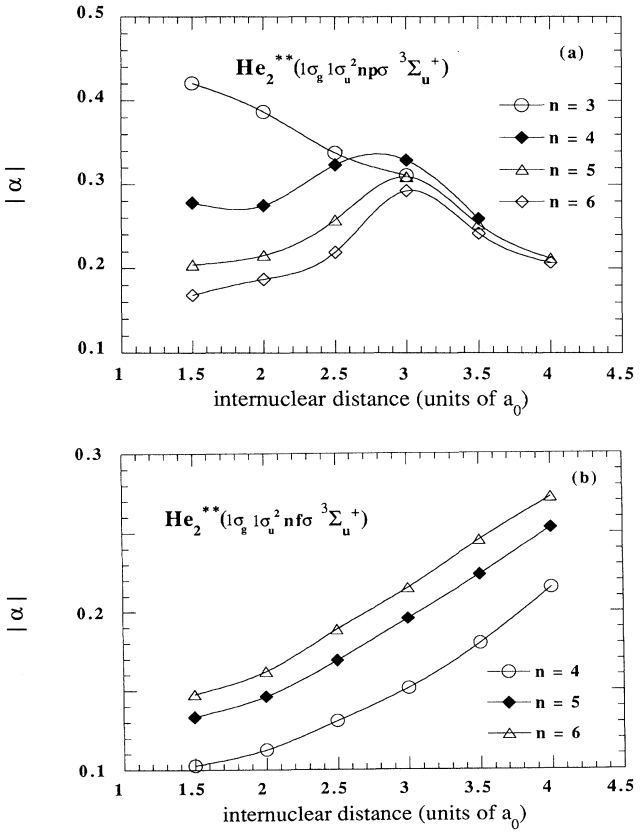

FIG. 5. Real part α_n of the quantum defect μ_n for the $np\sigma$ and $nf\sigma\ ^3\Sigma_u^+$ Rydberg series as a function of internuclear distance. (a) is the $np\sigma\ ^3\Sigma_u^+$ series and (b) the $nf\sigma\ ^3\Sigma_u^+$ series.

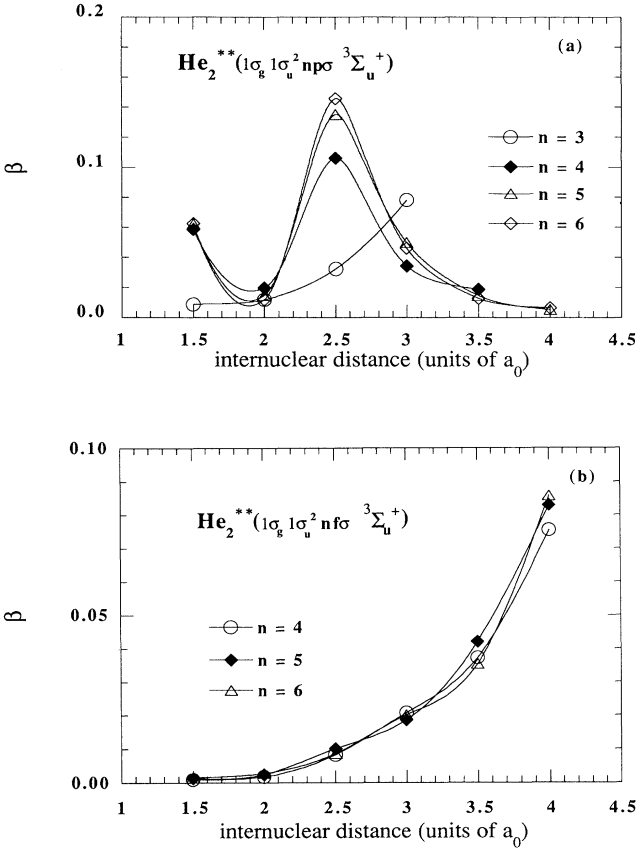

FIG. 6. Imaginary part β_n of the quantum defect μ_n for the $np\sigma$ and $nf\sigma\ ^3\Sigma_u^+$ Rydberg series as a function of internuclear distance. (a) is the $np\sigma\ ^3\Sigma_u^+$ series and (b) the $nf\sigma\ ^3\Sigma_u^+$ series.

TABLE XI. Calculated absolute energies, in hartrees, of the lowest-lying $^3\Sigma_u^+$ state of He_2^*. The energy of the $a\ ^3\Sigma_u^+$ state is compared with the MCSCF calculations of Sunil *et al.* [49], the SA-MCSCF/SOCI calculations of Yarkony [59], and the SOCI calculations of Konowalow and Lengsfield [60], at the internuclear separation $R = 2.0625a_0$. Our results are obtained by performing bound-state R-matrix scattering calculations.

Method	Energy
R matrix	−5.131 26
R matrix (method of Seaton)	−5.131 53
MCSCF	−5.138 47
SA-MCSCF/SOCI	−5.146 25
SOCI	−5.148 05

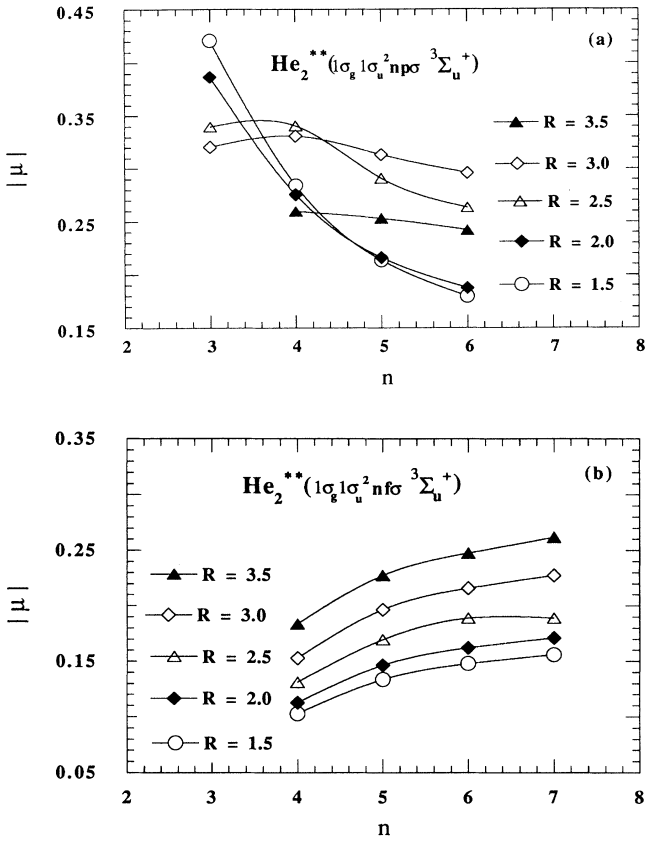

FIG. 7. Absolute magnitude of the quantum defect $|\mu|$ for the $np\sigma$ and $nf\sigma\ ^3\Sigma_u^+$ Rydberg series as a function of principal quantum number n. (a) is the $np\sigma\ ^3\Sigma_u^+$ series and (b) the $nf\sigma\ ^3\Sigma_u^+$ series.

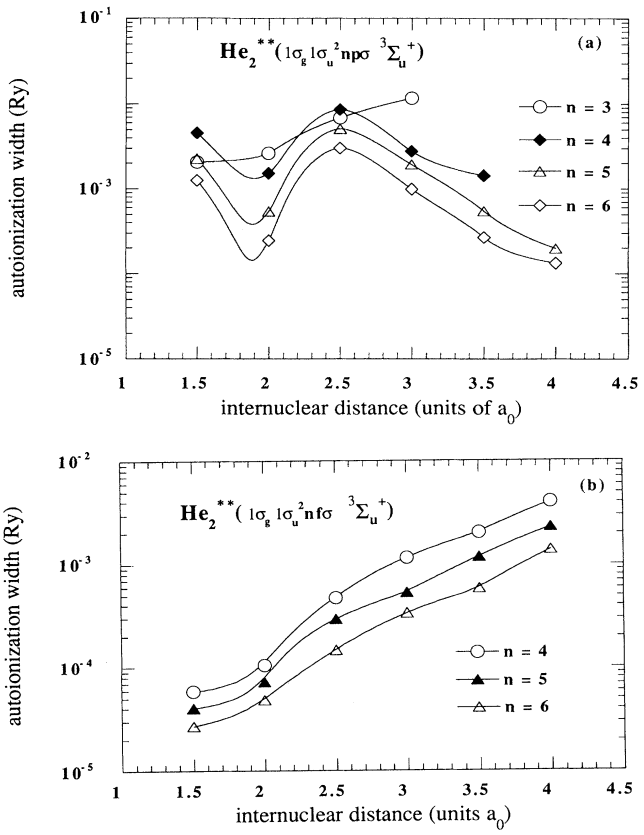

FIG. 8. Autoionization widths for the $np\sigma$ and $nf\sigma\ ^3\Sigma_u^+$ Rydberg series as a function of internuclear distance. (a) is the $np\sigma\ ^3\Sigma_u^+$ series and (b) the $nf\sigma\ ^3\Sigma_u^+$ series.

evaluating Rydberg bound states of molecules such as H_2, HeH, H_2^-, HF^-, and HCl^-.

Table XI provides comparison of our bound-state results, obtained from the close-coupling method with results of quantum chemistry calculations. The results are for the energy of the lowest-lying $a\ ^3\Sigma_u^+ He_2^*$ state at the internuclear distance of $R = 2.0625a_0$, a value close to that of the equilibrium geometry r_e. Included in Table XI is the result from the method of Seaton, as implemented by Sarpal *et al.* [27], together with our previous R-matrix result. This provides an indication of the effectiveness of this method and for the sake of completeness. Where necessary, for direct comparison with other authors, we have interpolated the appropriate potential-energy curves. Our absolute energies from both methods are in satisfactory agreement with the MCSCF calcula-

TABLE XII. Energies in hartrees, effective quantum number (n^*), and quantum defect ($n-n^*$), for the $He_2(1\sigma_g^2 1\sigma_u ns, nd\sigma$, and $ng\sigma\ ^3\Sigma_u^+)$ Rydberg bound states at internuclear distance $R = 1.5a_0$.

State	Energy	n^*	$n-n^*$
$2s$	−5.077 462	1.795 066	0.204 934
$3s$	−4.984 995	2.823 844	0.176 156
$3d\sigma$	−4.973 290	3.131 163	−0.131 163
$4s$	−4.956 444	3.826 250	0.173 750
$4d\sigma$	−4.952 125	4.093 893	−0.093 893
$5s$	−4.943 771	4.824 766	0.175 234
$5g\sigma$	−4.942 228	5.007 926	−0.007 926
$5d\sigma$	−4.941 706	5.074 891	−0.074 891
$6s$	−4.937 035	5.823 552	0.176 448
$6g\sigma$	−4.936 133	6.010 226	−0.010 226
$6d\sigma$	−4.935 883	6.065 255	−0.065 255

TABLE XIII. Energies in hartrees, effective quantum number (n^*), and quantum defect ($n-n^*$), for the $He_2(1\sigma_g^2 1\sigma_u ns, nd\sigma$, and $ng\sigma\ ^3\Sigma_u^+)$ Rydberg bound states at internuclear distance $R = 2.0625a_0$.

State	Energy	n^*	$n-n^*$
$2s$	−5.131 533	1.834 710	0.165 290
$3s$	−5.044 504	2.851 137	0.148 863
$3d\sigma$	−5.037 606	3.025 859	−0.025 859
$4s$	−5.016 617	3.856 336	0.143 664
$4d\sigma$	−5.014 332	3.994 447	0.005 553
$5s$	−5.004 186	4.857 474	0.142 526
$5d\sigma$	−5.003 146	4.981 280	0.018 720
$5g\sigma$	−5.002 919	5.009 622	−0.009 622
$6s$	−4.997 567	5.857 857	0.142 143
$6d\sigma$	−4.997 000	5.975 231	0.024 769
$6g\sigma$	−4.996 835	6.010 609	−0.010 609

TABLE XIV. Energies in hartrees, effective quantum number (n^*), and quantum defect ($n-n^*$), for the $He_2(1\sigma_g^2 1\sigma_u ns, nd\sigma$, and $ng\sigma\ ^3\Sigma_u^+$) Rydberg bound states at internuclear distance $R=2.5a_0$.

State	Energy	n^*	$n-n^*$
$2s$	−5.114 780	1.850 459	0.149 541
$3s$	−5.029 686	2.864 751	0.135 249
$3d\sigma$	−5.025 957	2.956 666	0.043 334
$4s$	−5.002 129	3.870 958	0.129 042
$4d\sigma$	−5.001 229	3.924 257	0.075 743
$5s$	−4.989 821	4.872 540	0.127 460
$5d\sigma$	−4.989 482	4.912 141	0.087 859
$5g\sigma$	−4.988 671	5.011 203	−0.011 203
$6s$	−4.983 256	5.873 045	0.126 955
$6d\sigma$	−4.983 093	5.906 453	0.093 547
$6g\sigma$	−4.982 596	6.011 468	−0.011 468

tions of Sunil *et al.* [48], the state averaged MCSCF–second-order CI (SA-MCSCF-SOCI) calculations performed by Yarkony [59], and the second-order configuration-interaction (SOCI) calculations of Konowalow and Lengsfield [60].

Presented in Tables XII–XIV are the results we have obtained for the bound states of He_2^* using the method of Seaton. This information on the electronic $He_2^*(1\sigma_g^2 1\sigma_u ns$, nd, and $ng\ ^3\Sigma_u^+$) Rydberg states is given for the bond lengths of 1.5, 2.0625, and $2.5a_0$, to illustrate the power of this quantum-defect technique.

The curves of Fig. 9 show how the energies of the $He_2^*(1\sigma_g^2 1\sigma_u ns\ ^2\Sigma_u^+$) Rydberg states vary with internuclear separation. The results are similar to the work of Ginter and Batino [61]. Finally, our numerical values of these energies for several separations are collected in Table XV.

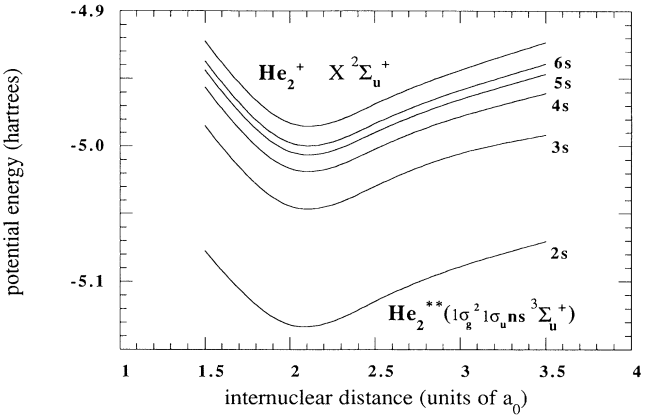

FIG. 9. $He_2(1\sigma_g^2 1\sigma_u ns\ ^3\Sigma_u^+$) Rydberg states as a function of internuclear distance, obtained from performing bound-state collision calculations using the method of Seaton. Correlated CI target wave functions obtained from natural orbital analysis of MCSCF-CASSCF calculations are used to represent the X and A states of the He_2^+ molecular ion.

IV. CONCLUSIONS AND FUTURE DIRECTIONS

Results have been presented on low-energy elastic scattering by electrons from He_2^+ molecular ions for the $^3\Sigma_u^+$ symmetry. These scattering calculations have enabled us to calculate the energies of several low-lying $^3\Sigma_u^+$ bound states of the He_2^* molecule at internuclear separations in the range $1.5–4.0a_0$. In addition we have presented *ab initio* calculations of the resonances widths for low-lying $np\sigma$ and $nf\sigma$ quasibound states with $^3\Sigma_u^+$ scattering symmetry. Our scattering results, using full CI target-state representations obtained from the natural orbitals generated by MCSCF-CASSCF calculations, give information on $^3\Sigma_u^+$ bound and continuum states of the e^--He_2^+ collision complex. We have calculated the bound and continuum electronic states of the helium dimer at this level of CI approximation, whereas other theoretical approaches tended to cater either to the bound or continuum states of the collision complex.

As an extension to this work we intend to investigate nuclear vibrational motion, using a nonadiabatic R-matrix approach [53]. Other scattering symmetries also will be studied. Future calculations are planned to employ a multistate approximation that includes other low-lying states of the He_2^+ target. We also plan to carry out *ab initio* studies of photoionization cross sections for several of the low-lying excited singlet and triplet states of the helium dimer.

ACKNOWLEDGMENTS

We thank Dr. Susan Branchett and Dr. Jonathan Tennyson for helpful discussions on the evaluation of bound states. The scattering computations were carried out on the Cray-X-MP/EA/4P/64 MW at the Minnesota Supercomputer Center. The MCSCF-CASSCF He_2^+ structure calculations were performed on the IBM 3090-600J using

TABLE XV. Energies in hartrees for the $He_2(1\sigma_g^2 1\sigma_u ns\ ^3\Sigma_u^+$) Rydberg states at selected bond separations.

R (units of a_0)	$2s$	$3s$	$4s$	$5s$	$6s$
1.5	−5.077 462	−4.984 995	−4.956 444	−4.943 771	−4.937 035
2.0	−5.131 842	−5.044 411	−5.016 468	−5.004 017	−4.997 388
2.0625	−5.131 533	−5.044 504	−5.016 617	−5.004 186	−4.997 567
2.5	−5.114 780	−5.029 686	−5.002 129	−4.989 821	−4.983 256
3.0	−5.089 141	−5.005 447	−4.978 037	−4.965 384	−4.958 580
3.5	−5.070 512	−4.991 725	−4.960 851	−4.946 623	−4.939 108

the ALCHEMY II codes [37], at the Cornell National Supercomputer Facility, a resource of the Center for Theory and Simulation in Science and Engineering at Cornell University, which receives funding by the National Science Foundation, New York State, the IBM Corporation, and members of the Corporate Research Institute. This work was completed during short term visits by C.J.G. and B.M.McL. to the Minnesota Supercomputer Institute. We thank the National Science Foundation, the Minnesota Supercomputer Institute, and the Science and Engineering Research Council in the United Kingdom, for their financial support during the course of this research. Finally, the Institute for Theoretical Atomic and Molecular Physics at the Harvard-Smithsonian Center for Astrophysics is funded by the National Science Foundation under Grant No. PHY324-88.

---

*Present address: IBM Almaden Research Center, 650 Harry Road, San Jose, CA 95120-6099.

[1] W. R. Gentry (private communication).
[2] B. J. Garrison, W. H. Miller, and H. F. Schaefer III, J. Chem. Phys. **59**, 3193 (1973).
[3] M. W. Müller, W. Bussert, M. W. Ruf, and H. Hotop, Phys. Rev. Lett. **59**, 2279 (1987).
[4] J. C. Hill, L. L. Hatfield, N. D. Stockwell, and G. K. Walters, Phys. Rev. A **5**, 189 (1972).
[5] B. M. McLaughlin, C. J. Gillan, P. G. Burke, and J. S. Dahler, Nucl. Instrum. Methods B **53**, 518 (1991).
[6] B. M. McLaughlin, C. J. Gillan, P. G. Burke, and J. S. Dahler, *Atomic and Molecular Physics,* edited by C. Cisneros, I. Alvarex, and T. J. Morgan (World Scientific, London, 1991), p. 161.
[7] J. S. Cohen, Phys. Rev. A **13**, 86 (1976); **13**, 99 (1976).
[8] R. J. Bieniek, M. W. Müller, and M. Movre, J. Phys. B **23**, 4521 (1990).
[9] M. W. Müller, W. Bussert, M. W. Ruf, H. Hotop, W. Meyer, and M. Movre, Z. Phys D **21**, 89 (1991).
[10] P. S. Julienne and F. H. Mies, J. Opt. Soc. Am. B **6**, 2257 (1989).
[11] J. Weiner, F. Masnou-Seeuws, and A. Giusti-Suzor, Adv. At. Mol. Opt. **26**, 209 (1990).
[12] A. Niehaus, Phys. Rep. **186**, 149 (1990).
[13] A. N. Klucharev and V. Vujnovic, Phys. Rep. **185**, 55 (1990).
[14] K. T. Gillen, Phys. Rev. A **39**, 2248 (1989).
[15] P. Monchicourt, P. Padel, D. Dubreuil, and J. J. Laucagne, Phys. Rev. A **40**, 1147 (1989); **40**, 6706 (1989).
[16] S. Lepp, A. Dalgarno, and R. McCray, Astrophys. J. **358**, 262 (1990).
[17] B. M. McLaughlin, P. Scott, and J. S. Dahler (unpublished).
[18] S. L. Guberman, *Physics of Ion-Ion and Electron-Ion Collisions,* edited by F. Brouillard and J. W. McGowan (Plenum, New York, 1983), p. 167.
[19] C. J. Gillan (unpublished).
[20] C. J. Gillan, O. Nagy, P. G. Burke, and L. A. Morgan, J. Phys. B **20**, 4585 (1987).
[21] J. Tennyson, C. J. Noble, and S. Salvini, J. Phys. B **17**, 905 (1984).
[22] J. Tennyson and C. J. Noble, J. Phys. B **18**, 155 (1985).
[23] I. Shimamura, C. J. Noble, and P. G. Burke, Phys. Rev. A **41**, 3545 (1990).
[24] S. E. Branchett and J. Tennyson, J. Phys. B **25**, 2017 (1992).
[25] B. K. Sarpal and J. Tennyson, J. Phys. B **25**, L49 (1992).
[26] J. Tennyson, J. Phys. B **21**, 805 (1988).
[27] B. K. Sarpal, S. E. Branchett, J. Tennyson, and L. Morgan, J. Phys. B **24**, 3685 (1991).
[28] M. J. Seaton, J. Phys. B **18**, 2111 (1985).
[29] P. N. Reagen, J. C. Browne, and F. A. Matsen, Phys. Rev. **132**, 304 (1963).
[30] I. Shavitt, *Modern Theoretical Chemistry: Vol. 3, Methods of Electronic Structure Theory,* edited by H. F. Schaefer III (Plenum, New York, 1977), p. 189.
[31] R. S. Mulliken and W. C. Ermler, *Diatomic Molecules: Results of Ab Initio Calculations* (Academic, New York, 1977); *Polyatomic Molecules: Results of Ab Initio Calculations* (Academic, New York, 1981).
[32] A. Kahn and K. D. Jordan, Chem. Phys. Lett. **128**, 368 (1986).
[33] A. C. Wahl and G. Das, *Modern Theoretical Chemistry: Vol. 3, Methods of Electronic Structure Theory,* edited by H. F. Schaefer III (Plenum, New York, 1977), p. 51.
[34] R. E. Farren and K. P. Kirby (private communication).
[35] A. D. McLean, *Proceedings of the Conference on Potential Energy Surfaces in Chemistry,* edited by W. A. Lester, Jr. (IBM, San Jose, 1971), p. 87.
[36] C. J. Noble, Daresbury Laboratory Report No. DL/SCI/TM33T, 1982 (unpublished).
[37] The ALCHEMY I and II suite of programs were originally developed by P. S. Bagus, B. Liu, A. D. McLean, M. Yoshime, and B. Lengsfield III.
[38] S. E. Branchett and J. Tennyson, Phys. Rev. Lett. **64**, 2889 (1990).
[39] C. J. Noble (private communication).
[40] C. Bloch, Nucl. Phys. **4**, 87 (1957).
[41] P. J. A. Buttle, Phys. Rev. **162**, 719 (1967).
[42] K. L. Baluja, P. G. Burke, and L. A. Morgan, Comput. Phys. Commun. **27**, 299 (1982).
[43] C. J. Noble and R. K. Nesbet, Comput. Phys. Commun. **33**, 399 (1984).
[44] H. Michels, Natl. Bur. Stand. (U.S.) Tech. Note **438**, 109 (1967).
[45] A. Metropoulos, C. A. Nicolaides, and R. J. Buenker, Chem. Phys. **114**, 1 (1989).
[46] M. Barat, D. Dhuico, R. Francois, R. McCarroll, R. D. Piacentini, and A. Salin, J. Phys. B **5**, 1343 (1972).
[47] A. Metropoulos, Z. Naturforsch. **44a**, 683 (1989).
[48] N. Yu and W. H. Wing, Phys. Rev. Lett. **59**, 2055 (1987).
[49] K. K. Sunil, J. Lin, H. Siddiqui, P. E. Siska, K. D. Jordan, and R. Shephard, J. Chem. Phys. **78**, 6190 (1983).
[50] N. Yu, W. H. Wing, and L. Adamowicz, Phys. Rev. Lett. **62**, 253 (1989).
[51] N. Yu and L. Adamowicz, J. Chem. Phys. **90**, 4392 (1989).
[52] C. W. Bauschlicher, Jr., H. Partridge, and D. Ceperley, Chem. Phys. Lett. **160**, 183 (1989).
[53] B. K. Sarpal, J. Tennyson, and L. Morgan, J. Phys. B **24**, 1851 (1991).
[54] M. J. Seaton, Rep. Prog. Phys. **46**, 167 (1983).

[55] J. Tennyson and C. J. Noble, Comput. Phys. Commun. **33**, 421 (1984).
[56] J. Tennyson (private communication).
[57] T. Gorczyca and D. W. Norcross, Phys. Rev. A **42**, 5132 (1990).
[58] T. Gorczyca and D. W. Norcross, Phys. Rev. A **45**, 140 (1992).
[59] D. R. Yarkony, J. Chem. Phys. **90**, 7164 (1989).
[60] D. D. Konowalow and B. H. Lengsfield III, J. Chem. Phys. **87**, 4000 (1987).
[61] M. L. Ginter and D. S. Batino, J. Chem. Phys. **52**, 4469 (1969).
[62] J. G. Mass, N. P. F. B. van Asselt, P. J. C. H. Nowark, J. Los, S. D. Peyerimhoff, and R. J. Buenker, Chem. Phys. **17**, 217 (1976).
[63] B. Liu, Phys. Rev. Lett. **27**, 1251 (1971).
[64] K. P. Huber and G. Herzberg, *Molecular Spectra and Molecular Structure IV: Constants of Diatomic Molecules* (Van Nostrand, New York, 1979).
[65] M. L. Ginter and D. S. Ginter, J. Chem. Phys. **48**, 2284 (1968).